Water-water interfaces

E.M. Blokhuis[1], N.J.H. Boon[2], H.T.M. van den Ende[3], Z. Krumer[4], B. Nienhuis[5], R. van Roij[2], M.C. Schaafsma[6], and R.H. Tromp[7]

[1] *Leiden Institute of Chemistry, University of Leiden*
[2] *Institute for Theoretical Physics, University of Utrecht*
[3] *Physics of Complex Fluids, University of Twente*
[4] *Debye Institute, University of Utrecht*
[5] *Institute for Theoretical Physics, University of Amsterdam*
[6] *FOM Institute AMOLF, Eindhoven*
[7] *NIZO Food Research BV, Ede*

Abstract:

NIZO food research is an independent contract research company that employees 200 workers which assist food and ingredient companies. One of the key objectives in food research is the understanding under which conditions water-water emulsions are stable. It is often desirable from an environmental point of view to replace organic solvents by water. Also, the increased demand for low-fat food products leads to the question to what extent water-water emulsions can replace water-oil emulsions. The NIZO research question posed to the physics community is therefore to find surfactant-like molecules that sit at the water-water interface. The surfactant-like molecules may then be tailored (1) to make sure that there is a repulsion between emulsion droplets (by adding charge, etc) necessary for stability, (2) to change the rigidity of the emulsion droplet's surface. The formulation of a theoretical framework to understand the properties of the water-water interface is therefore our main goal.

1   Company Introduction

NIZO food research is an independent contract research company. About 200 employees (Staff: 60 fte graduates, 75 fte others) assist food and ingredient companies to be more profitable by developing and applying competitive technologies. NIZO works on the basis of confidential projects with the international dairy, food & beverage, ingredients and biotech industries. Key areas are:

• Innovation (flavour, texture, health),

• Cost reduction (process efficiency, ingredient replacement, test productions),

• Responsible entrepreneurship (food safety & quality, sustainable processing, evidence based health claims).

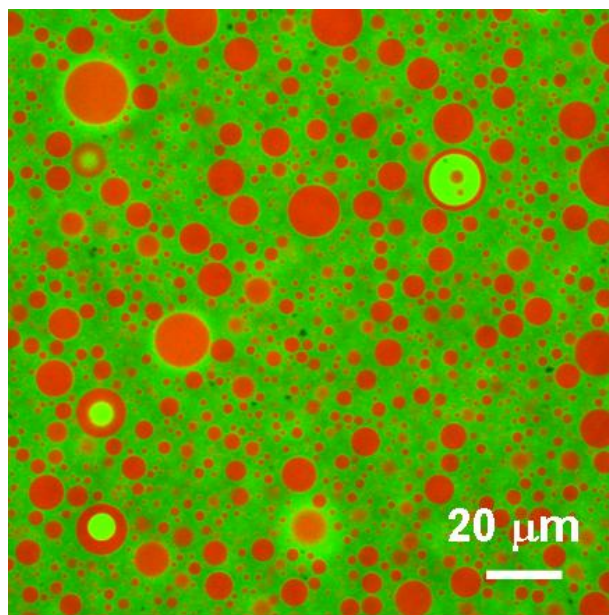Turn over revenue for 2009 was 20,000,000 Euro.

Figure 1: Water-water emulsion, from a phase separated aqueous solution of 10% fish gelatin (non-gelling), and 10% dextran (200 kDa). Red: gelatin-rich; green: dextran-rich.

2 Problem description

Interfaces between phases of coexisting thermodynamically incompatible aqueous solutions are called water-water interfaces. Their most common occurrence is between phase separated aqueous polymer solutions, such as solutions containing polysaccharides and proteins. The water-water interface in that case is found between the co-existing protein-rich and polysaccharide-rich solution. An important difference from interfaces between phase separated polymer blends (polymer mixtures without solvent), arises from the accumulation of solvent at the interface. This accumulation of solvent at the interface lowers the interfacial tension. The interfacial tension of water-water interfaces is extremely low (typically a few μN/m or less). These interfaces are therefore highly deformable and difficult to investigate by classical methods (e.g the Wilhelmy plate method). Water, salt and, in the case of polydisperse polymers, low molar mass fractions of the polymers can freely diffuse across the interface.

From a scientific point of view, water-water interfaces, as well as solvent-solvent interfaces in general, are interesting because of their extremely low interfacial tension and because of the fact that the interfacial width may be able to respond to curvature by expelling or absorbing water. The sensitivity of the interfacial profile to the presence of a wall (through wetting) or curvature may explain the peculiar observation of the co-existence of curvature in water-water emulsions. Examples are the long-time stability of a broad size distribution of droplets in density-matched water-water emulsions (Fig. 1), and the relatively complicated, apparently stable shape of water-water emulsion droplets squeezed in a confined geometry (Fig. 2). The particular case of an aqueous solvent has the extra dimension of (partial) permeability for salts and the subsequent possibility of Donnan potentials across the interface. The partial permeability makes water-water interfaces comparable to semi-permeable dialysis membranes.

The industrial relevance of a deep understanding of water-water interfaces arises from the close link with structuring and functionalizing high-water systems. High water systems have favorable properties, such as a low environmental impact and a low caloric value.
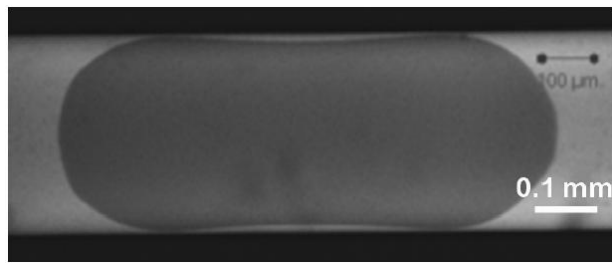
Figure 2: Droplet of dextran-rich phase surrounded by gelatine-rich phase in a capillary tube. The gelatin-rich phase wets the wall of the capillary tube.

Relevance to industry

The interface between two aqueous polymer solutions is interesting from both a scientific as well as a practical point of view. The tendency towards environmentally friendly industrial processes in which water takes the place of organic solvent is increasing their occurrence in practical systems. The demand for low fat processed food makes more urgent the question to what extent a water-water interface can be given the same properties as oil-water interfaces. A third area in which the feasibility of the application of water-water interfaces is emerging is in systems for controlled release of pharmaceuticals in the human body. The key question with respect to applications of water-water interfaces in food systems is therefore: how can the water-water interface be controlled and tailored in order to give it the properties desirable in food systems. Examples of these properties are stability, preferential curvature and permeability to specific compounds. The basic mechanisms might be borrowed from cell walls in living systems. Ideally, design rules would become available for polymers, co-polymers or particles which have a favourable free energy when located at the water-water interface. Their presence may reduce the interfacial tension even further, but more importantly, they may stabilize the interface by imparting an interfacial rigidity or a preferential curvature [1]. All these effects would slow down coalescence in a water-water emulsions and bring fully water-based systems with useful sensory and shelf-life properties closer to practical application.

Problem solving strategy

We have formulated three sub-topics that are worked out in the next sections:

• Extending the Broseta model to asymmetric polymer mixtures,
• Designing surfactant-like molecules that adsorb at the water-water interface,
• Shape of droplets in a capillary (see Fig. 2).

3   Extending the Broseta model to asymmetric polymer mixtures

In this sub-topic, we investigate the theoretical framework by Broseta *et al.* [2, 3, 4] for a mixture of two polymers in solution. In their case, the two polymers are chosen to be identical in size and composition but mutually repellent. This leads to a phase separation between two phases, one rich in polymer of type A and the other rich in polymer of type B; see Fig. 3. The Figure shows that because of the symmetry of the model, the composition through the interface is symmetric and there is no preferential curvature toward either phase. Our goal is to extend the theoretical framework by Broseta *et al.* [2] in which the symmetry is broken and map out the consequences for the direction of the preferential curvature.
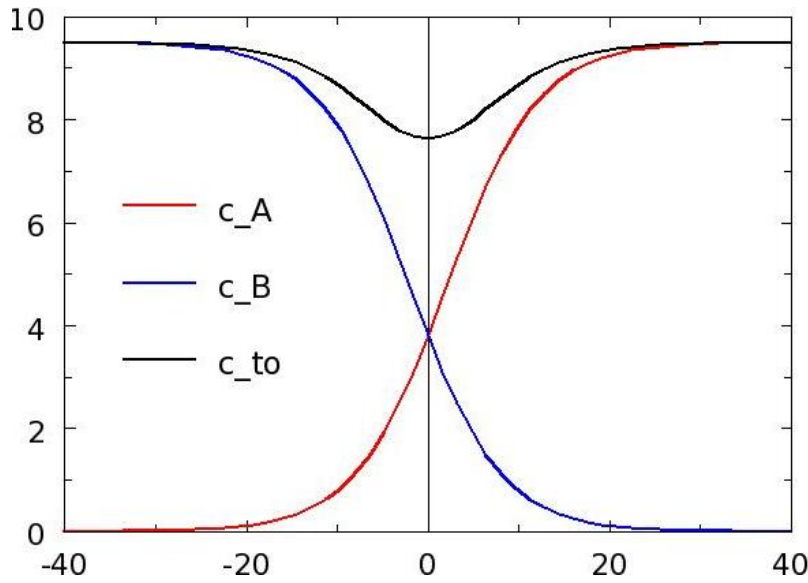
Figure 3: Typical monomer concentration profiles as a function of the height z (in nm) in the interfacial region between a polymer A-rich phase on the right and a polymer B-rich phase on the left. $c_{\text{tot}} = c_A + c_B$ is the total monomer concentration and shows a clear depletion in the interfacial region of about 20 nm wide.

First, we sketch the physical background of the free energy used by Broseta *et al.* [2]. This should provide us with insight in possible routes to extend their model. The derivation of Broseta *et al.* [2] starts with the Flory Huggins model [5] for an isotropic polymer melt consisting of two polymer types of equal length N. We denote the volume fractions of type A and type B as $\phi_A = \phi$ and $\phi_B = 1 - \phi$. Then,

$$\frac{F_{\text{FH}}(\phi)}{V k_B T} = \frac{1}{a^3} \left[\frac{\phi}{N} \ln(\phi) + \frac{(1-\phi)}{N} \ln(1-\phi) + \chi \phi (1-\phi) + K \right]. \tag{1}$$

where a is the dimension of the lattice. The usual Flory parameter χ stands for the interaction between the two polymer types, and $K = 0.024$ is a constant [3] related to the osmotic pressure.

The Flory-Huggins model is used by Broseta *et al.* [2] for a mixture of two polymers in solution well above the overlap concentration (semi-dilute solution). In that situation the **blob model** can be used to describe the solution [6]. We consider the whole volume consisting of 'blobs' of dimension ξ (the correlation length) with each 'blob' either containing polymer of type A or type B; see Fig. 4a. The free energy is then of the Flory-Huggins type with a replaced by ξ and the polymer length N replaced by the number of blobs, $N_b = N/(c \xi^3)$:

$$\frac{F_{\text{blob}}(\phi, c)}{V k_B T} = \frac{1}{\xi^3} \left[\frac{\phi}{N_b} \ln(\phi) + \frac{(1-\phi)}{N_b} \ln(1-\phi) + u \phi (1-\phi) + K \right]. \tag{2}$$

where u now describes the interaction between blobs of type A and B. It is essential to keep in mind that both the correlation length $\xi = \xi(c)$ and $u = u(c)$ will depend on the total monomer concentration c [6]:

$$\xi(c) = \bar{\xi} \left(\frac{c}{\bar{c}} \right)^{-3/4} \qquad \text{and} \qquad u(c) = \bar{u} \left(\frac{c}{\bar{c}} \right)^{0.275}, \tag{3}$$

where the bar denotes the respective value at a reference concentration $c = \bar{c}$, for which we shall take the bulk concentration.
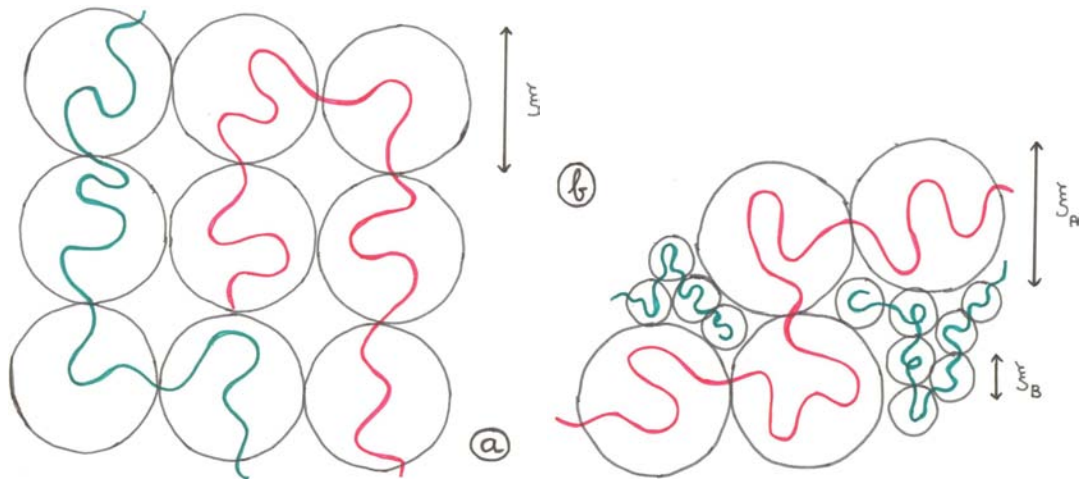
Figure 4: Sketch of the blob-model by de Gennes [6] for a polymer solution containing two types of polymers. Left: symmetric case, where the correlation length ξ is the same for for both polymer species. Right: asymmetric case, where the correlation lengths ξ_A and ξ_B are different.

Broseta *et al.* [2] now use the above blob free energy model for an isotropic polymer mixture to describe the interfacial region between the demixed polymer phases. This is achieved by allowing $\phi(z)$ and $c(z)$ to be height dependent and by adding squared gradient terms to the free energy:

$$
\begin{aligned}
\frac{F[\phi(z), c(z)]}{A\, k_{\mathrm{B}} T} \;=\; & \int_{-\infty}^{\infty} dz \left[\frac{\phi}{N_b\, \xi^3}\, \ln(\phi) + \frac{(1-\phi)}{N_b\, \xi^3}\, \ln(1-\phi) + \frac{u}{\xi^3}\, \phi\,(1-\phi) \right. \\
& \left. + \frac{K}{\xi^3} + \frac{\phi'(z)^2}{24\, \xi\, \phi} + \frac{\phi'(z)^2}{24\, \xi\,(1-\phi)} + \frac{c'(z)^2}{24\, \xi\, c^2} \right].
\end{aligned}
\tag{4}
$$

The two squared gradient terms involving $\phi_A = \phi$ and $\phi_B = 1 - \phi$ can be combined, but we have left them as is, so that we can easily generalize to the non-symmetric case. In that case we allow ξ_A and ξ_B to differ; see Fig. 4b. This leads to the following expression for the free energy

$$
\begin{aligned}
\frac{F[\phi(z), c(z)]}{A\, k_{\mathrm{B}} T} \;=\; & \int_{-\infty}^{\infty} dz \left[\frac{\phi}{N_{b,A}\, \xi_A^3}\, \ln(\phi) + \frac{(1-\phi)}{N_{b,B}\, \xi_B^3}\, \ln(1-\phi) + \frac{u}{\xi_{\mathrm{eff}}^3}\, \phi\,(1-\phi) \right. \\
& \left. + \frac{K}{\xi_{\mathrm{eff}}^3} + \frac{\phi'(z)^2}{24\, \xi_A\, \phi} + \frac{\phi'(z)^2}{24\, \xi_B\,(1-\phi)} + \frac{c'(z)^2}{24\, \xi_{\mathrm{eff}}\, c^2} \right],
\end{aligned}
\tag{5}
$$

where we have defined an effective correlation length as

$$
\frac{1}{\xi_{\mathrm{eff}}^3} = \frac{1}{2}\left(\frac{1}{\xi_A^3} + \frac{1}{\xi_B^3} \right).
\tag{6}
$$

The free energy in Eq.(5) is the main result of this section. It can now be used to calculate concentration profiles and curvature parameters such as the preferential curvature and the surface rigidity. This needs to be carried out in future work. Here, we limit ourselves to the determination of the phase diagram as a function of the asymmetry ratio, $r = \xi_A^3 / \xi_B^3$. Fig. 5 shows the result. On the left the experimental phase diagram is shown for the
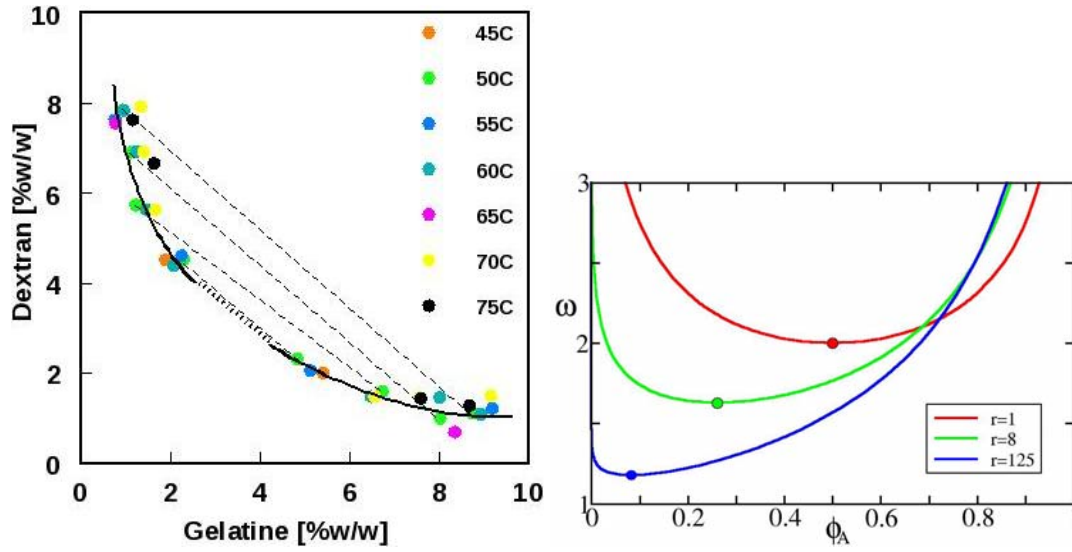
Figure 5: Polymer mixture phase diagrams. Left: experimental phase diagram of the gelatine/dextran mixture for different temperatures. Right: Calculated phase diagram for several asymmetry ratios, $r = \xi_A^3/\xi_B^3 = 1$, 8, and 125.

gelatine/dextran mixture for a number of different temperatures, whereas on the right the calculated phase diagram is shown using the expression for the free energy in Eq.(5). The x-axis shows the volume fraction of the A-rich phase, ϕ_A (the volume fraction of the B-rich phase necessarily equals $\phi_B = 1 - \phi_A$) and the y-axis is the reduced parameter $\omega = \bar{N}_b \bar{u}$ [2]. The shift in the location of the critical point towards lower ω signifies the fact that it is easier to obtain phase separation when the two polymers differ in size. One further observes that the volume fraction of the polymer A-rich phase, having the larger blob size, decreases significantly.

4   Designing surfactant-like molecules that adsorb at the water-water interface

We consider a water-water emulsion with a polymer A-rich phase and a polymer B-rich phase. The interfacial profile between the two phases can be described by the modified Broseta model [2] as depicted in Fig. 3.

Since we aim to stabilize the emulsion by adding surfactant-like polymers to the interface, we investigate the affinity of a single polymer molecule near the interface by calculating its free energy as a function of the distance z to the interface. To this end, we model the polymer as a flexible Gaussian chain with N Kuhn segments of length b and sum the energies of all the segments given the position of the center of mass of the polymer z_{CM}. The energy of a single segment at a distance z to the interface, is estimated as:

$$E_{segm}(z) = k_B T \left[\varepsilon_{SA} \phi_A(z) + \varepsilon_{SB} \phi_B(z) + \varepsilon_{SW} \left(1 - \phi_A(z) - \phi_B(z) \right) \right] + \text{const} \qquad (7)$$

$$= k_B T \left[(\varepsilon_{SA} - \varepsilon_{SW}) \phi_A(z) + (\varepsilon_{SB} - \varepsilon_{SW}) \phi_B(z) \right] + \text{const}, \qquad (8)$$

where the polymer volume fraction ϕ_α is defined as:

$$\phi_\alpha = \rho_\alpha N_\alpha b^3, \qquad (9)$$

with ρ_α the number density of polymers of type α and N_α their length. Note that b is the length of a Kuhn segment of the surfactant molecule. The dimensionless affinities ε_{SA},
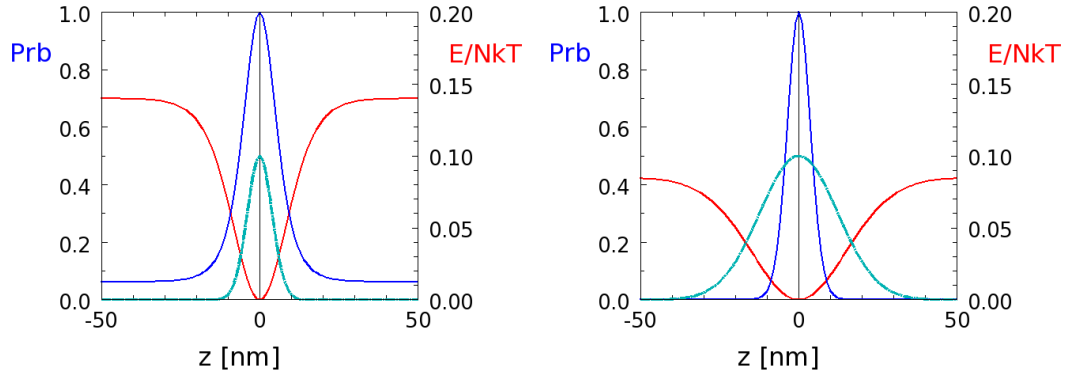
Figure 6: The red curve represents the energy per segment of a surfactant molecule as a function of its distance to the interface at $z=0$, for $\phi_A^\infty = \phi_B^\infty = 0.8$. The blue curve represents the probability to find a surfactant molecule at a distance z from the interface. The cyan curve represents the segment density profile of a surfactant molecule located at its favourite position. Left: $N = 20$, right: $N = 200$.

ε_{SB} and ε_{SW} represent the interaction energies of the surfactant-like molecule with respect to polymer A, polymer B and water, respectively. In this simple picture of a surfactant molecule, the energy of a single segment depends linearly on the number density of the polymers in both phases: $E_{\text{segm}}(z) = k_B T \left[c_A \rho_A(z) + c_B \rho_B(z) \right] + const$ where the coefficients $c_\alpha = (\varepsilon_{S\alpha} - \varepsilon_{SW}) N_\alpha b^3$ combines several characteristics of the system. Hence an asymmetry of the problem can be introduced via ρ_α or c_α. Here, we use the density profile to introduce asymmetry in the problem and keep $c_A = c_B$. The energy of the surfactant molecule itself is given by:

$$E(z_{\text{CM}}) = \int_{-\infty}^{\infty} dz \, n(z; z_{\text{CM}}) \, E_{\text{segm}}(z) , \tag{10}$$

where $n(z; z_{\text{CM}}) dz$ is the number of segments between z and $z + dz$ inside the surfactant polymer:

$$n(z; z_{\text{CM}}) = \frac{N}{\left(2\pi R_0^2\right)^{1/2}} \exp\left(-\frac{(z - z_{\text{CM}})^2}{2R_0^2}\right), \tag{11}$$

where $R_0 = \sqrt{b^2 N/3}$. Combining these last two equations yields:

$$E(z_{\text{CM}}) = \sqrt{\frac{3N}{2\pi b^2}} \int_{-\infty}^{\infty} dz \, \exp\left(-\frac{3 (z - z_{\text{CM}})^2}{2b^2 N}\right). \tag{12}$$

The corresponding probability to find a surfactant molecule a distance z_{CM} from the interface, is given by the Boltzmann factor:

$$P(z_{\text{CM}}) = P_0 \exp\left(\frac{-E(z_{\text{CM}})}{k_B T}\right). \tag{13}$$

To obtain generic results from this model, we approximate the density profiles of the polymer A-rich and polymer B-rich phase by:

$$\phi_A(z) = \frac{\phi_A^\infty}{2} \left(1 + \tanh\left(\frac{z - z_{\text{dl}}/4}{z_{\text{th}}}\right)\right), \tag{14}$$
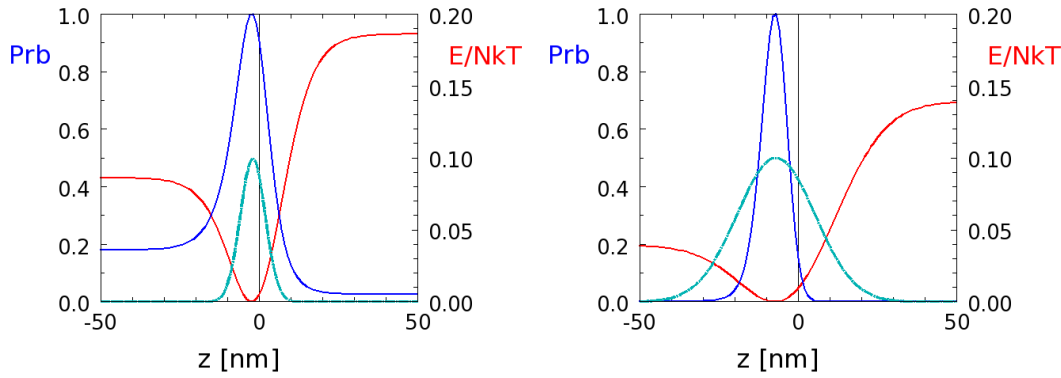
Figure 7: The same as in Fig. 6 but now for the asymmetric case: $\phi_A^\infty = 0.8$, $\phi_B^\infty = 0.7$. Again, left: $N = 20$, right: $N = 200$.

and

$$\phi_B(z) = \frac{\phi_B^\infty}{2}\left(1 - \tanh\left(\frac{z + z_{\mathrm{dl}}/4}{z_{\mathrm{th}}}\right)\right), \tag{15}$$

where $z_{\mathrm{dl}} = 8$ nm represents the width of the depletion layer between the two phases and $z_{\mathrm{th}} = 10$ nm the thickness of the interface between the two phases. The segment length of the surfactant is set to $b = 1.5$ nm and both affinity differences are set to: $(\varepsilon_{SA} - \varepsilon_{SW}) = (\varepsilon_{SA} - \varepsilon_{SW}) = 1$ (in units of $k_B T$). First we consider the symmetric case with $\phi_A^\infty = \phi_B^\infty = 0.8$. In Fig. 6, the energy $E/Nk_B T$ per segment of a surfactant molecule has been plotted versus its distance from the interface for a surfactant length of $N = 20$ (left) and $N = 200$ (right). Also, the corresponding probability to find the surfactant-like molecule at a distance z from the interface has been plotted. For reference, also the segment density profile of the surfactant molecule in its most favourable position has been plotted. For $N = 20$ all segments fit in the depletion zone and the energy gain is considerably: $0.14\ k_B T$. For $N = 200$, however, the segment distribution is much wider, not all the segments fit in the depletion zone and due to that the energy gain per segment is lower: $0.08\ k_B T$. The center of mass distribution is still a bit sharper because the total energy gain for $N = 200$ is still larger.

In Fig. 7 the results are given for the asymmetric case $\phi_A^\infty = 0.8$, $\phi_B^\infty = 0.7$. The same effects are visible as in the symmetric case in Fig. 6. Moreover, due to the difference in bulk concentration of polymer A and polymer B, the most favourable position of the surfactant shifts towards the polymer B-rich phase, because the segments try to avoid the polymer A-rich phase due to its lower water content. This shift increases with increasing surfactant length as one can conclude from a comparison of the left and the right graph.

To investigate the influence of the surfactant length on its affinity for the interface in more detail, we calculated $E(z = \infty) - E_{\min}$, which reflects the energy gain of a surfactant molecule at the interface with respect to the polymer A-rich phase, and $E(z = -\infty) - E_{\min}$, which reflects the gain with respect to the polymer B-rich phase, as a function of the surfactant length N. The results have been plotted in Fig. 8. For $\phi_A^\infty = \phi_B^\infty$ both energy gains are equal (left) but when $\phi_A^\infty > \phi_B^\infty$ there is a considerable difference for long surfactant molecules (right). This is caused by the tendency to avoid the polymer A-rich phase, which implies for large molecules that they are strongly pushed away from the interface and hardly feel the depletion zone anymore.
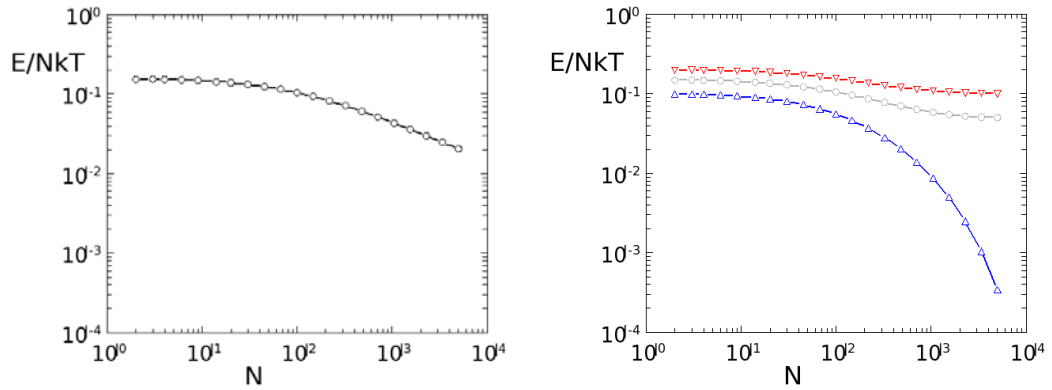
Figure 8: Energy gain per segment E/Nk_BT at the interface with respect to the bulk phases as a function of the number of segments N. Left: $\phi_A^\infty = \phi_B^\infty = 0.8$, right: $\phi_A^\infty = 0.8$, $\phi B^\infty = 0.7$. The energy gain with respect to the polymer A-rich phase is given in red, the gain with respect to the polymer B-rich phase in blue, the gray curve represents the average of the blue and red curves.

4.1 Electrostatic energy of partially charged surfactant polymers

Let us consider a surfactant polymer with N_G chargeable groups. The surfactant can either be in one of the polymer-rich bulk phases, where it is surrounded by all other polymers, or in the interfacial region, where the density of polymer is lower. The surfactant interacts with other polymers, which can be described by defining interaction energies for each available polymer species. This interaction, however, is not considered here. The aim is to find a relation to describe the difference in the surfactant's electrostatic (self-)energy between the bulk phase and the interface due to slight changes in electrolyte properties.

Self-Energy

If we assume that the charged monomers on a surfactant polymer chain can effectively be described by charged spheres with radius a, the electrostatic self-energy of the entire polymer chain follows from DLVO-theory [7],

$$U_{\text{self}}(\mathbf{r}) = \frac{\lambda_b(\mathbf{r})}{1 + \kappa a},$$ (16)

where $\lambda_b(\mathbf{r}) = \beta e^2/\epsilon(\mathbf{r})$ is the Bjerrum length which will depend on the local value of the dielectric constant $\epsilon(\mathbf{r})$, $\beta = 1/k_BT$ is the inverse temperature, and κ is the Debye screening parameter. Now, a rough estimate on the radius of a charged monomer and the screening parameter tells us that $\kappa a \ll 1$, so that we can safely ignore this term in the remaining calculations. The difference in water concentration between the polymer-rich phase and the interface is about 2%, which is small. Nevertheless, this may still have some influence on the electrostatic self-energy of the polymer since a changing water concentration will affect the local value of the dielectric constant. As a very rough estimate, we assume that the dielectric constant decreases linearly from $\epsilon_w \simeq 80$ for pure water to approximately $\epsilon \simeq 0$ for pure polymers,

$$\epsilon(\mathbf{r}) = \epsilon_w \eta(\mathbf{r}),$$ (17)

where $\eta(\mathbf{r})$ is the local water volume fraction. This variation in the dielectric constant has immediate consequences for the Bjerrum length, therefore a small difference $\Delta\eta$ (which is typically around 2%) in the water volume fraction between the polymer-rich bulk phase

and the interface will lead to

$$\lambda_{b,\text{interface}} = \lambda_{b,\text{bulk}}(1 - \Delta\eta). \tag{18}$$

One may shift the self-energy such that it vanishes in the bulk (since this does not affect the properties of the system) and rewrite it as

$$\beta U_{\text{self}} = \begin{cases} 0 & \text{in the bulk}, \\ -N_{\text{G}}\dfrac{\lambda_{b,\text{bulk}}\Delta\eta}{2a} & \text{in the interface}. \end{cases} \tag{19}$$

The increase in water concentration leads to an increased tendency of the polymers to move to the interfacial region. As presently shown, the amount of polymer that actually moves to the interface is bounded by the electrostatic repulsion between the polymers.

Interaction Energy

The electrostatic interaction energy of the charged monomers in the interface volume is described by a very basic Donnan-equilibrium model. From Boltzmann theory we know that the local density of positive and negative ions is described by [7]

$$\rho_+(\mathbf{r}) = \rho_s\, e^{-\beta e\psi(\mathbf{r})}, \tag{20}$$

$$\rho_-(\mathbf{r}) = \rho_s\, e^{+\beta e\psi(\mathbf{r})}, \tag{21}$$

where $\psi(\mathbf{r})$ is the local electrostatic potential, e the elementary charge and ρ_s is the density of added salt ions to the system. The net local density of ion charges therefore becomes

$$\rho_{\text{ion}}(\mathbf{r}) = e\rho_+(\mathbf{r}) - e\rho_-(\mathbf{r}) = -2\,\rho_s\,\sinh(\beta e\psi(\mathbf{r})). \tag{22}$$

The polymer charge density is related to the local number density n_{surf} of surfactant polymers via

$$\rho_{\text{charges}}(\mathbf{r}) = N_{\text{G}}\, n_{\text{surf}}(\mathbf{r}). \tag{23}$$

The Donnan potential now follows from charge neutrality in the interface, $\rho_{\text{ion}}(\mathbf{r}) = \rho_{\text{charges}}(\mathbf{r})$, such that

$$\beta e\psi_{\text{Donnan}}(\mathbf{r}) = \text{arcsinh}\left(N_{\text{G}}\frac{n_{\text{surf}}(\mathbf{r})}{2\rho_s}\right). \tag{24}$$

The interaction energy therefore follows from $\frac{1}{2}\rho_{\text{charges}}(\mathbf{r})\,e\,\psi_{\text{Donnan}}(\mathbf{r})$. Like we already assumed, the concentration of surfactant polymers in the bulk will in general be too small to generate a substantial interaction energy between its charges. Furthermore, we assume the Donnan potential in the interface to be of the order of $1\,k_{\text{B}}T$ such that we can approximate $\text{arcsinh}(x) \approx x$. Then one finds for the interaction energy

$$\beta U_{\text{interaction}}(\mathbf{r}) = \begin{cases} 0 & \text{in the bulk}, \\ N_{\text{G}}^2\dfrac{n_{\text{surf}}}{2\rho_s} & \text{in the interface}, \end{cases} \tag{25}$$

where n_{surf} now has become the number density of surfactant polymers in the interface. One may wonder if including the (indirect) influence of the entropy of the ions to this interaction energy would be important. This could in general be the case. Nevertheless, here it is assumed that the amount of added salt to the system is enough to make the local ion densities not to be influenced strongly by charged objects, such that $\rho_\pm(\mathbf{r}) \approx \rho_s$ (i.e. we are in the linear regime of the Poisson-Boltzmann equation.) Therefore, the ion-entropic penalty for a high concentration of surfactant polymers in the interface layer is assumed to be small.
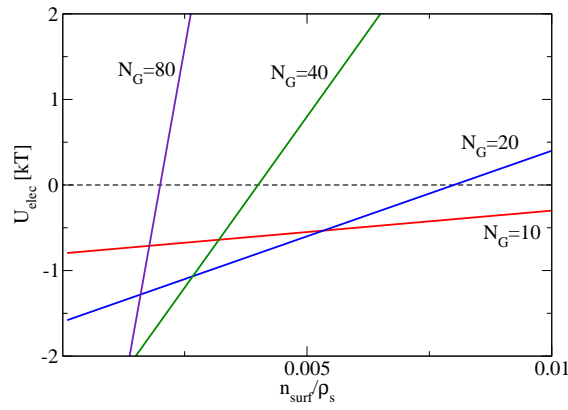
Figure 9: The electrostatic energy per surfactant polymer as a function of the number density of this polymer in the interface layer relative to the salt concentration concentration, for different values N_G, and $\Delta\eta = 0.02$, and $\lambda_{b,\text{bulk}}/a = 8$.
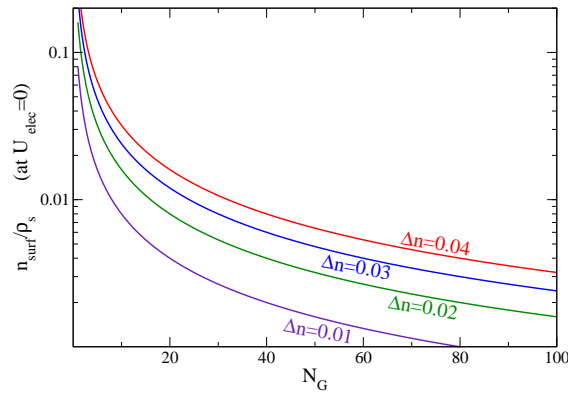

Figure 10: The critical interface surfactant concentration n_{surf} (relative to salt concentration ρ_s) at which the electrostatic energy crosses the bulk value 0, as a function of the number of charged monomers N_G. Plotted are results for multiple water concentration differences $\Delta\eta$ between bulk and interface, using $\lambda_{b,\text{bulk}}/a = 8$.

If one combines both the result for the self-energy and the interaction energy, one finds that the total electrostatic energy U_{elec} is given by

$$\beta U_{\text{elec}} = \begin{cases} 0 & \text{in the bulk}, \\ -N_G \dfrac{\lambda_{b,\text{bulk}}\Delta\eta}{2a} + N_G^2 \dfrac{n_{\text{surf}}}{2\rho_s} & \text{in the interface}. \end{cases} \tag{26}$$

For the parameters $\Delta\eta = 0.02$, $\lambda_{b,\text{bulk}}/a = 8$ and different values for N_G, Fig. 9 shows the electrostatic energy as a function of the surfactant concentration. What is immediately clear is that at very low surfactant concentrations in the interface, each new surfactant polymer gains considerable energy by moving to the interface. This gain is initially the largest for the surfactant polymers with the most charged groups; they bind the strongest to the interface. As the interface gets populated, the interaction energy begins to become important. The energy gain decreases, as we see from the upward slopes in Fig. 9. The surfactant concentration where it is no longer favourable to add additional surfactant to the interface is expected to be roughly around the point where the electrostatic energy in Fig. 9 crosses zero. This critical surfactant concentration is shown as a function of the number of charged groups, for several choices for $\Delta\eta$, in Fig. 10. It can be seen that the critical

surfactant concentration decreases as the number of charged groups increases. So in order to prepare a good surfactant, one is tempted to choose only a few charged groups on each surfactant molecule. Nevertheless, the number of charged groups should also not be too small, as the surfactant then probably is not able to bind strong enough to the interface anymore. Therefore, the number of charges on the surfactant molecule should be fine tuned. Furthermore the results also suggests that increasing the salt concentration can help to obtain higher concentrations of surfactant in the interface.

5 Shape of droplets in a capillary

The experimental data available to the team included a picture in which a gelatin- and dextran-rich phase alternate over the length of a glass capillary; see Fig. 2. As the gelatin-rich phase wets the wall, the dextran phase forms droplets. The droplet is elongated in the direction of the capillary, and is separated from the gelatin-rich fluid by two almost semi-spherical caps. In between, the droplet does not follow the cylindrical shape of the capillary, but is slightly squeezed: it has a waist.

The interface between two phases takes a shape that minimizes its free energy. Since this free energy is usually proportional to the area of the interface, a typical interface has minimal area, given certain constraints such as the volume of the phases which its separates. This implies (see below) that the total curvature (the trace of the curvature tensor) is constant over the surface and equal to the difference of pressure between the two sides divided by the surface tension [8].

This seems inconsistent with the picture: in the caps the total curvature is equal to $2/R$, where R is the radius of the capillary. If the droplet would in the middle fill the intersection of the capillary, its surface would be cylindrical, and have total curvature $1/R$, as it is curved only in one direction. The true curvature is slightly different: the radius is slightly smaller, increasing the curvature, and the curvature in the longitudinal direction of the capillary, is negative. These two effects contribute in opposite directions, but their magnitude is relatively small compared to $1/R$. This leaves a mismatch between the curvature at the cap and at the waist of close to a factor 2.

We consider the following mechanisms to explain this mismatch:

- **Disjoining pressure:** The Van der Waals forces between the glass and the different water phases results in a repulsive pressure between the interface and the glass wall inversely proportional to the cube of the distance. Could this possibly be more effective in the middle of the droplet?

- **Trapping:** As a result of the history of the formation of the droplet, some gelatin-rich fluid may be trapped between the droplet and the capillary wall. This would be a transient effect, as this fluid is squeezed out by the excess pressure in the droplet. The question is if it exists long enough to remain during the observation.

- **Curvature dependence of the surface tension:** If the surface tension is not constant on the surface of the droplet but depends on e.g. the curvature, this may affect the shape of the droplet [9].

The first analysis is to see of the effects mentioned are strong enough to have the observed effect.

- **Disjoining pressure:** The mismatch in pressure is of the order of σ/R, where σ is the interfacial tension, and R the radius of the capillary. Here $\sigma \simeq 0.1~\mu$ N/m and $R \simeq 0.15$ mm. The disjoining pressure is of the form A/d^3, where d is the distance of the
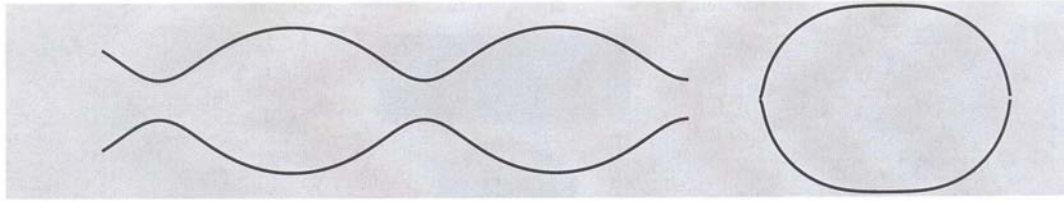
Figure 11: Left: periodic solution of the shape equation. Right: droplet with singular points at the tips.

interface to the wall, and A some proportionality constant related to the Hamaker constant [7], which is typically of the order of 10^{-21} J. From the picture in Fig. 2 we conclude that $d \simeq 0.01$ mm near the waist of the droplet. Substitution of the numbers makes the disjoining force too small by some 6 orders of magnitude.

- **Trapping:** Assuming that the mismatch in pressure is actually a difference between the pressure in the gelatin-rich phase well outside the droplet and that trapped between the droplet and the capillary. On the scale of the effect it looks like flow between parallel plates. The volume trapped per unit of circumference is 3×10^{-8} m^2, The pressure gap is approximately 7×10^{-4} N/m^2, spanned over 0.1 mm, leaves a pressure gradient of 7 N/m^3. Flux per unit length between parallel plates is $\Phi = d^3 \nabla p / (12\eta)$, where d is the distance between the plates ($\simeq 1$ μm here), and η the viscosity. The time for the liquid to be squeezed out thus comes to 10^7 s, assuming that the viscosity is a few times that of water. This is indeed longer than the observation time.

- **Curvature dependence of the surface tension:** Here we have no theory to guide us, but since the mismatch in curvature is close to a factor two, this should be compensated with a difference in interfacial tension of also a factor two. It is hard to imagine that a curvature dependence on this scale can affect the surface tension that much.

The shape of the droplet is governed by the minimization of the free energy, keeping constant the droplets volume. We assume rotational symmetry around the axis of the capillary, and denote the radius of the droplet as $r(x)$ with x the coordinate along the capillary.

$$ 0 = \frac{\delta}{\delta r} \int dx \left[2\pi \sigma r(x)(1 + r'(x)^2)^{1/2} - \pi \Delta p \, r(x)^2 + V(r) \right], \qquad (27) $$

in which Δp is a Lagrange multiplier to control the volume, σ is the surface tension, and $V(r)$ is the free energy of the interaction with the capillary, or disjoining potential [7]. Eventually Δp will play the role of pressure jump between the inside and outside of the droplet. The Euler-Lagrange equations following from this variation are:

$$ 0 = 2\pi \sigma \left[-r(x)r''(x)(1 + r'(x)^2)^{-3/2} + (1 + r'(x)^2)^{-1/2} \right] - 2\pi \Delta p \, r(x) + V'(r). \qquad (28) $$

The term proportional with $2\pi\sigma$ can be recognized as $r(x)$ times the total curvature. To see quickly the nature of the solutions it is simplest to integrate the differential equation numerically; see Fig. 11.

The gray area in Fig. 11 is the interior of the capillary. The typical solutions are periodic in x representing a series of not quite separated droplets, shown on the left. By tuning precisely the integration constants one can obtain a droplet, shown on the right. In the coordinates $r(x)$ and x the droplet of course has a singular point at the tip of the cap. Even though the disjoining force is taken into account, the droplets are everywhere convex. One could question if this can be altered by changing the disjoining potential.

It is easy to verify that the following quantity

$$C = 2\pi\,\sigma\,r(x)(1 + r'(x)^2)^{-1/2} - \pi\,\Delta p\,r(x)^2 + V(r)\,, \qquad (29)$$

does not depend on x. In dynamical terms (x representing time) it is a constant of the motion. This implies that for each droplet solution, $r'(x)^2$ can be expressed as a single valued function of $r(x)$ and the constant C. This excludes the possibility of a droplet with a waist. This shows convincingly, aside from the strength of the effect, that disjoining force cannot explain the shape of the droplet, *irrespective of the shape of the disjoining potential*, even with e.g. a potential minimum at close proximity of the wall.

The tentative conclusion is that the effect of the shape of the droplet is a non-equilibrium effect, caused by the history of the formation of the droplet. This implies that different droplets of the same aspect ratio will not have the same shape, but have a distribution of waist sizes. Presumably this prediction can be verified or falsified by further observations.

We have not fully decided that the non-equilibrium shapes are long enough stable against diffusion of the gelatin through the dextran droplet. And we also have not verified if curvature dependence of the interfacial tension would at least in principle (aside from the possible strength of the effect) allow droplets that are locally concave.

6   Summary

One of the key objectives in food research is the understanding under which conditions water-water emulsions are stable. The NIZO research question posed to the physics community is to find surfactant-like molecules that may be tailored to ensure stability of the emulsion and to give the emulsion surface the properties desirable in food systems. The following three topics were addressed:

• We investigated the theoretical framework by Broseta *et al.* [2] which provides monomer concentration profiles through the interfacial region. We have extended the Broseta model to asymmetric polymer mixtures (see Eq.(5)), in which the two polymer species may differ in length and molecular properties. This is necessary to obtain information on the preferred curvature to either phase and provide insight in modelling asymmetric monomer concentration profiles. The phase diagram was calculated and it was shown that it is easier to obtain phase separation when the two polymers differ in size.

• We investigated the properties a surfactant-like molecule should have in order to adsorb at the water-water interface. From the monomer concentrations obtained in the Broseta model (see Fig. 3) it is clear that the water-water interface is characterized by a region in which polymer is depleted. This leads to the observation that a polymer molecule that repels both polymer species A and B, would prefer to be in the interfacial region. This requirement is quite different than that of ordinary surfactant molecules that need to be amphiphilic in nature. We have shown that this mechanism turns out to work as long as the surfactant-like polymer is not too short or too long (the radius of gyration should be comparable to the width of the depletion layer). Furthermore it was shown that putting a modest amount of charge on the surfactant-like polymer enhances adsorption due to the favourable interaction with the water surrounding. The presence of too much charge destroys this effect because of the Coulomb repulsion between charges.

• We have addressed the peculiar observation of the co-existence of curvature in water-water emulsion droplets squeezed in a confined geometry (Fig. 2). We showed that the van der Waals forces between the capillary wall and the droplet's surface are too small to explain the observed curvature difference. Also, it is hard to imagine that a possible curvature dependence of the surface tension could play a role on the scale of mm's. It

was therefore tentatively concluded that the effect is a non-equilibrium effect, caused by the history of the formation of the droplet. This implies that different droplets of the same aspect ratio will not have the same shape, but have a distribution of waist sizes. This prediction should be verified by further observations.

References

[1] W. Helfrich, *Z. Naturforsch.* **28C**, 693 (1973).

[2] D. Broseta, L. Leibler, L.O. Kaddour, and C. Strazielle, J. Chem. Phys. **87**, 7248 (1987).

[3] D. Broseta, L. Leibler, and A. Lapp, Europhys. Lett. **2**, 733 (1986); D. Broseta, L. Leibler, and J.-F. Joanny, Macromolecules **20**, 1935 (1987).

[4] R.H. Tromp, Chapter 9 in *Structure and Functional Properties of Colloidal Systems*, Surfactant Science Series **146**, Ed. Hidalgo-Alvarez, CRC Press, Boca Raton (2010).

[5] P.F. Flory, *Principles of Polymer Chemistry*, (Cornell University Press, Ithaca, 1953).

[6] P.G. de Gennes, *Scaling Concepts in Polymer Physics* (Cornell University Press, Ithace, 1979).

[7] D.F. Evans and H. Wennerström, *The Colloidal Domain*, 2nd Ed (Wiley-VCH, New York, 1999).

[8] J.S. Rowlinson and B. Widom, *Molecular Theory of Capillarity* (Clarendon, Oxford 1982).

[9] E.M. Blokhuis, Chapter 3 in *Surface and Interfacial Tension*, Surfactant Science Series **119**, Ed. S. Hartland, Dekker, New York (2004).